Added mass of rising bubble approaching to solid wall – numerical studies

Jan Zawala

Jerzy Haber Institute of Catalysis and Surface Chemistry Polish Academy of Sciences, ul. Niezapominajek 8, 30-239 Krakow, Poland

Corresponding author: nczawala@cyfronet.pl

Abstract: The numerical approach for determination of influence of deformation of the gas bubble (radius 0.74 mm) on added mass coefficient in (i) steady-state conditions and (ii) during approach to the horizontal wall, is proposed. It is shown that the bubble deformation can be tuned numerically (within the range 1.06 - 1.88) via proper variations of the Laplace pressure, without changing the bubble radius. Influence of the bubble deformation on its motion parameters is discussed and compared to theoretical predictions regarding the bubble drag coefficient and Reynolds number. Moreover, the approach allowing determination of the added mass of rising bubble, on the basis of variations in fluid kinetic energy, is described. It is shown that calculated added mass variations strongly depends on the interplay between (i) the bubble deformation ratio and (ii) its rising velocity. This effect is especially important for added mass of a gas bubble approaching a solid wall, because it can affect the kinetics of drainage of the separating liquid film formed under dynamic conditions, when Re >> 1.

Keywords: bubble, collision, added mass, liquid film, deformation, Laplace pressure, simulation

1. Introduction

Behaviour of bubbles in viscous fluid is of interest in many areas of fundamental physics and engineering where bubble dynamics is critical for optimization of a variety of engineered processes (Sangani et al., 1991). Gas-liquid contacting is one of the most common and important phenomena encountered in environmental applications, the chemical process industry, the petroleum industry, and mineral processing (Kulkarni and Joshi, 2005). For pure liquids, where the liquid/gas interface is free of adsorbed molecules, it is well established that the motion of the bubble is influenced mainly by bubble size, density difference between liquid and gas phases, and liquid viscosity. Immediately after formation in unbounded fluid the bubble accelerates due to the action of buoyancy and gradually reaches terminal (constant) velocity. For constant bubble size and invariable density and viscosity of the liquid, the surface tension is the most crucial factor affecting the bubble shape and rising velocity. Levich (1962) in his famous, classical book wrote that: "*(...) The greater the surface tension of the liquid, the less pronounced is the deformation of the drop. The velocity of fall, therefore, is higher for particles which have greater surface tension and become less flattened (...)*". Although he wrote about drops, this conclusion is valid also for the gas bubble, because the density difference between inner and outer phases is the only dissimilarity. The Levich's conclusion about higher rigidity of the bubble against liquid flow, causing smaller deformations of a bubble surface, is a consequence of higher Laplace pressure, which increases proportionally to the surface tension of the liquid.

Any motion of a fluid induced by a body moving through (bubble, for example) is associated with a certain amount of kinetic energy (T). For an accelerating body, increasing the velocity (u) causes an increase in T and, consequently, the energy that must be supplied to the fluid per unit time (dT/dt). In the simplest case of inviscid, idealized potential flow, this additional work is associated with the drag experienced by the body, $(-F_D \cdot u)$, equal to kinetic energy changes, where F_D is the drag force. This

"added drag" can be related to the so-called added mass because the drag force has the same dimensions as the force required to accelerate the mass of the body (Brennen, 1982). The concept of added mass was derived theoretically for an ideal, unbounded fluid having no resistance to shear stress (Milne-Thomson, 1968). In the case of real, viscous fluid, the additional drag term related to fluid viscosity has to be considered. The moving body experiences an additional steady drag as a consequence of the work necessary to balance the steady rate of energy dissipation in viscous fluid. For steady-state motion (which is rectilinear) the drag and viscous energy dissipation in unbounded fluid should be constant (Zawala, 2016). When the bubble approaches to the obstacle this situation changes significantly - the added mass increases (Milne-Thomson, 1968; Zawala and Dabros, 2013; Klaseboer et al., 2014). The rate of added mass increase, related to the hydrodynamic interactions between the bubble and solid surface, is of crucial importance for kinetic of the bubble collision, bouncing and drainage of the separating liquid film formed between interacting interfaces. All of the existing models of added mass variations are valid only for very low Reynolds numbers (*Re*), under assumption of potential flow. Moreover, added mass variations were evaluated for spherical bodies. The added mass changes, however, can be much more complicated for higher *Re*. Due to the fact that in majority of technological and applied processes the *Re* are much greater than 1, knowledge about influence of the bubble motion parameters on the added mass variations is very important. This was underlined recently by Simcik and Ruzicka (2013), who shown the influence of approaching bubble deformation on its added mass coefficient variations, calculated for the bubble acceleration.

The present work describes the numerical studies on influence of the bubble deformation on its motion parameters and added mass variations in steady-state conditions and during approach to a horizontal no-slip wall. After Levich (1962), the deformation of the bubble of constant size is tuned via changing the Laplace pressure values (pressure inside a bubble) in a liquid of physical properties (density, viscosity) equal to the properties of water. Influence of the bubble shape deformation on drag coefficient, terminal velocity and added mass is calculated for free rise. The calculations, validated on the basis of literature data, are mainly aimed to discuss the rate of increase of added mass of a bubble approaching to a horizontal wall, the parameter of crucial importance for kinetics of drainage of the liquid film formed under dynamic conditions (Klaseboer et al., 2014).

2. Methods

2.1. Governing equations and computational domain

Modeling of a bubble in liquid was performed on the basis of numerical simulations (*Gerris* software), implementing finite volume solvers on a quad/octree adaptive grid together with a volume of fluid (VOF) interface tracking method and automatic mesh generation with adaptive mesh refinement according to a hierarchical tree-based discretization approach (Popinet, 2009; Fuster et al., 2009). A spatial discretization and numerical scheme used to solve the governing equations in the form (Popinet, 2009):

$$\rho \left[\frac{\partial \mathbf{u}}{\partial t} + (\mathbf{u} \cdot \nabla)\mathbf{u} \right] = -\nabla p + \nabla \cdot (2\mu \mathbf{Q}) + \sigma \kappa \delta_s \mathbf{n} \tag{1}$$

$$\nabla \cdot \mathbf{u} = 0 \tag{2}$$

was described in detail in (Popinet, 2003; Popinet, 2009; Fuster et al., 2009). Eqs. 1-2 describe the conservation of momentum and mass of an incompressible, variable density liquid with deformation tensor **Q** defined as:

$$\mathbf{Q} = \frac{1}{2}(\nabla \mathbf{u} + (\nabla \mathbf{u})^T) = 0 \tag{3}$$

where $\mathbf{u} = [u, v, w]$ is the fluid velocity vector, ρ is the local density of the fluid, μ is the local viscosity of the fluid (water or air), p is a pressure, t is time, σ is surface tension, δ_s is a Dirac distribution function (expressing the fact that the surface tension term is concentrated at the interface), while κ and **n** are the curvature and normal unit vector to the interface, respectively.

The calculations were performed in the computational domain, which was a liquid column of height 100 mm and radius L equal to 2 or 10 mm (see Fig. 1), described by two-dimensional, cylindrical coordinate system. The bubble interface was reproduced and tracked using VOF approach. More details about the discretization parameters, mesh size and discretization algorithms can be found in (Zawala,

2016). Slip boundary conditions were assumed at the cylinder sidewalls, while the top liquid/solid interface was fixed as no-slip. Initially, for $t = 0$, the center of spherical gas bubble of arbitrary chosen radius $R = 0.74$ mm was set 5 mm above the bottom column wall at its symmetry axis. The density and viscosity of the liquid and gas corresponded to water and air, respectively (i.e., $\rho_l = 1000$ kg/m³ and $\mu_l = 1 \times 10^{-3}$ Pa·s in case of water and $\rho_a = 1.3$ kg/m³ and $\mu_a = 18 \times 10^{-6}$ Pa·s for air). The surface tension of liquid was tuned properly to obtain different Laplace pressure values, hence various bubble deformation degrees - this effect will be discussed in details further.
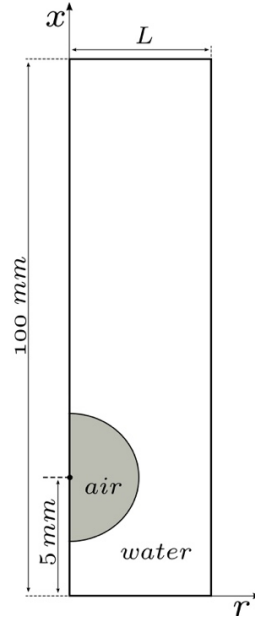
Fig. 1. Geometry of the computational domain

The total kinetic energy of the system of volume Ω, i.e. energy of fluid motion induced by the rising bubble (T) was calculated as (Ceschia and Nabergoj, 1978):

$$T = 0.5 \int_{\Omega} \rho \mathbf{u}^2 d\Omega \tag{4}$$

The rate of viscous dissipation of energy in the system (D) was calculated as (Bird et al, 2007):

$$D = \mu \int_{\Omega} \left\{ 2\left[\left(\frac{\partial u}{\partial x}\right)^2 + \left(\frac{\partial v}{\partial r}\right)^2 + \left(\frac{v}{r}\right)^2 \right] + \left(\frac{\partial u}{\partial r} - \frac{\partial v}{\partial x}\right)^2 - \frac{2}{3}\left(\frac{\partial u}{\partial x} + \frac{1}{r}\frac{\partial rv}{\partial r}\right)^2 \right\} d\Omega \tag{5}$$

The projected area of the rising bubble (A), used for estimation of the drag coefficient was evaluated as:

$$A = \pi R_v^2 R_h^2 \tag{6}$$

where R_v and R_h is the horizontal and vertical radius of the deformed bubble, respectively. The drag force (F_D) acting at the bubble in steady-state conditions (after the moment, when terminal velocity was established) was calculated according to the equation:

$$F_D = \frac{D}{u_b} \tag{7}$$

where u_b was the bubble terminal velocity. Having F_D values for the bubble with various degrees of deformation it was possible to calculate the drag coefficient (C_D) as:

$$C_D = \frac{2 \cdot F_D}{A \cdot \rho_l \cdot u_b^2} \tag{8}$$

The bubble deformation ratio (χ) in steady-state conditions was calculated as:

$$\chi = \frac{R_h}{R_v} \tag{9}$$

2.2. Bubble deformation tuning

In order to calculate influence of the bubble deformation (χ) on added mass variations, the Levich observation was used in the applied numerical approach (Levich, 1962). The radius of the bubble was

kept constant during all calculations, however, due to proper variations of the Laplace pressure values (pressure inside the bubble), the bubble deformation could be tuned, keeping all other physical parameters of the liquid and hydrodynamic boundary conditions at the liquid/gas interface constant. The liquid/gas interface was slip i.e. completely mobile, independently on the bubble deformation degree. The influence of gradually increasing Laplace pressure values on the bubble shape deformation, during free rise under steady-state conditions (terminal velocity) is illustrated in the Fig. 2. There are shown calculated bubble outlines (shapes). The detailed values on the Laplace pressure and corresponding bubble deformation values are given in Table 1, together with the values of the bubble terminal rise velocity. It has to be underlined here that deformation of the bubble could be tuned also by changing the bubble's equivalent radius. However, the simulated motion of bubbles of significantly different dimensions would be difficult to compare and would require the algorithm of modification of the size of the computational domain and computational mesh refinement. By changing the pressure values, only, and keeping the R_b constant, it was possible to use constant volume of the computational domain, what allowed convenient results comparison and made the numerical calculations stable and converge.

Table 1. Values of numerically tuned Laplace pressure and corresponding bubble deformation and velocity (L = 2 mm)}

	Laplace pressure [Pa]	χ	u_b [cm/s]
1	54	1.88	20.0
2	68	1.81	22.9
3	95	1.68	24.5
4	135	1.56	27.6
5	189	1.43	30.5
6	270	1.35	33.5
7	541	1.22	40.0
8	1351	1.10	43.9
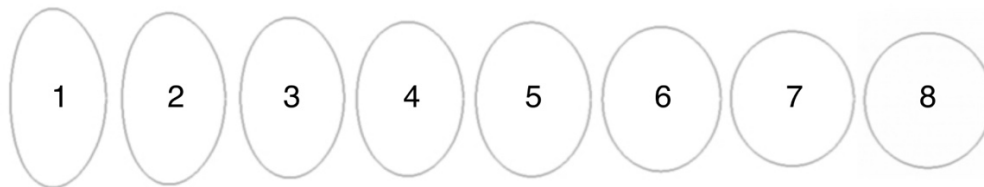
Fig. 2. Numerically reproduced shapes of the bubble of R_b = 0.74 mm with different Laplace pressure, rising in pure water, under steady-state conditions (with terminal velocity)

3. Results and discussion

As seen in Table 1 and corresponding snapshots presented in Fig. 2, the bubble deformation during free rise under steady-state conditions decreases with increasing Laplace pressure, while the bubble terminal velocity follows opposite trend. The effect reproduced in numerical simulations is, therefore, consistent with the Levich's conclusion (Levich, 1962).

Fig. 3 presents variations in the total kinetic energy associated with the bubble motion (Eq. 4) as well as corresponding variations of χ for the bubble of different Laplace pressure values rising in liquid (L = 2 mm). Both the T and χ are presented in Fig. 3 as a function of time. As seen at t = 0 bubble is motionless (T = 0) and spherical (χ = 1). The kinetic energy as well as deformation increases with time and start to be constant, i.e. the bubble reaches its terminal (constant) velocity. As could be expected, and already shown in Table 2, the highest bubble deformation is associated with the lowest value of the Laplace pressure. In turn, the final value of T reached for steady state conditions, (after bubble acceleration period and u_b establishment) is the highest for the lowest bubble deformation (i.e. when the

Laplace pressure is high enough to prevent the bubble from deformation by the counter-flow of the liquid, keeping the bubble almost spherical).
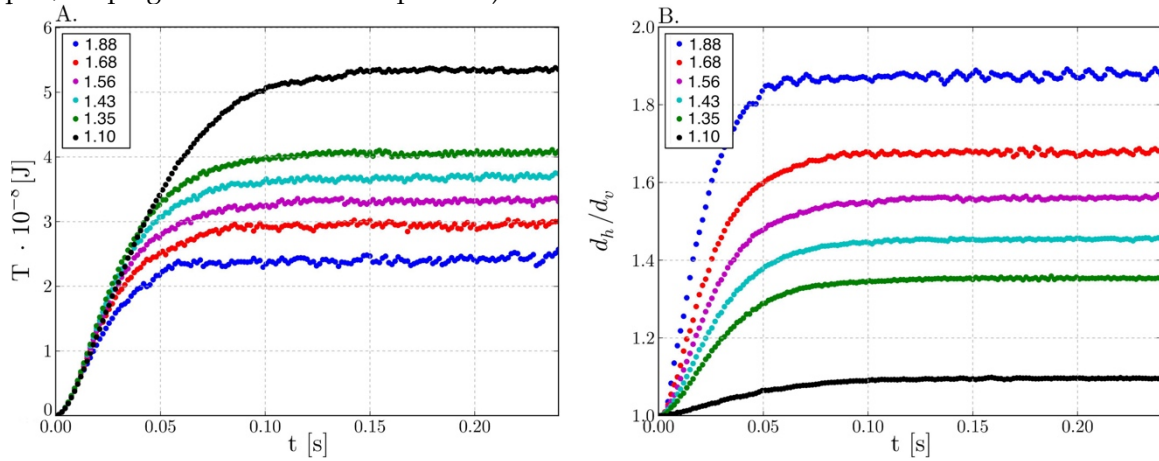
Fig. 3. Variations of (A) the total kinetic energy and (B) the bubble deformation during rise in liquid column of L = 2 mm (numbers in the legend correspond to the eventual values of the bubble deformation ratio)

The bubble terminal velocities (u_b) as well as T values calculated for steady-state conditions (as an average for the period where both values were constant in time) as a function of the bubble deformation ratios are presented in Fig. 4. The data obtained for L = 2 and 10 mm are presented there as points, while the dashed lines are fitted linear regressions. As was already mentioned above, both the bubble terminal velocity and kinetic energy decreases with decreasing Laplace pressure what, in turn, is related to the χ increase. In addition, significant difference between the data calculated for L = 2 and 10 mm can be noted. For similar value of the bubble deformation ratio, the bubble terminal velocity is lower for L = 2 mm comparing to 10 mm. Similar effect can be seen for T values (Fig. 4B). This significant discrepancy between velocity of the bubble rising in tube of different sizes should be attributable to the so-called wall effect (Clift et al., 1978; Malysa, 1992; Khrishna et al., 1999; Mukundakrishnan et al., 2007), which was present in the considered system, despite the slip boundary conditions applied at the column side walls. As was shown by Clift et al. (1978) the resistance coefficient correction λ, defined as a ratio of particle velocity in infinite fluid to its velocity in bounded fluid, depends on the ratio of bubble diameter to tube diameter ($S = 2R_b/L$) and can be expressed as:

$$\frac{1}{\lambda} = (1 - S^2)^{1.5} \tag{10}$$

Khrishna et al. (1999) showed that the wall effect does not affect the motion of a bubble if $S < 0.125$. In our experiments, for L = 10 mm the S = 0.074, so the condition for unbounded liquid was met. However, for L = 2 the S was much higher and equal to 0.37, what indicated that for the narrower tube the bubble motion was affected by the wall vicinity. In the case of L = 10 mm there was no influence of the side wall presence on the bubble motion. It is worth mentioning here that for L = 10 mm and the Laplace
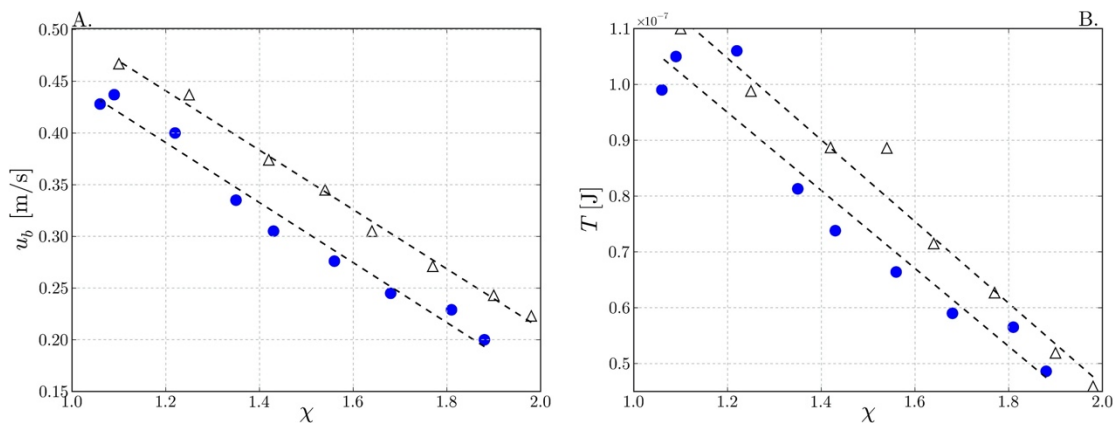
Fig. 4. Comparison of the bubble (A) terminal velocity and (B) kinetic energy associated with the bubble motion as a function of deformation, after establishment of the steady-state conditions - L = 2 mm full circles, L = 10 mm open triangles

pressure value corresponding to the real case of the bubble rising in water of surface tension 72.4 mN/m, both the bubble terminal velocity and the deformation was in excellent agreement with the corresponding values observed experimentally (Kosior et al. 2011), i.e. the χ = 1.54 and u_b = 34.3 cm/s. Good agreement between simulated and experimental results indicates that, indeed, the wall effect in the case of L = 10 mm can be neglected. As seen in Fig. 4 influence of the wall effect for L = 2 mm is constant and independent on the bubble deformation. The linear regressions (dashed lines) fitted to the data for both L values are parallel, what means that the wall effect is scalable and can be considered by introduction of the proper scaling factor. In this particular case the scaling factor is equal to ca. 0.8.

Fig. 5 presents the numerically calculated deformation of the bubble as a function of the Weber number (We), i.e the dimensionless number expressing the measure of the relative importance of the fluid's inertia compared to its surface tension, which can be expressed as:

$$We = \frac{2R_b \rho_l u_b}{\sigma} \tag{11}$$

where σ is an interfacial tension of the liquid/gas interface, given as $\sigma = 0.5 \cdot \Delta P \cdot R_b$. The ΔP is the Laplace pressure. The values of the We are compared in Fig. 5 to the relation estimated on the basis of experimental data by Legendre et al. (2012), who measured the bubble rising velocity and deformation in ultra clean water. He gave the following simple equation, which connects the bubble deformation with We values in water for the χ up to 3:

$$\chi = (1 - 0.140625 \cdot We)^{-1} \tag{12}$$

In addition, in Fig. 5 there are shown the data calculated theoretically by Klaseboer et al. (2011), who, on the basis of BEM simulations of potential flow with viscous effects, elaborated a model allowing prediction of terminal velocity of the bubble of different sizes. The terminal velocity values of the bubble of radius ranging between 0.6 - 2.2 mm given by this model (Klaseboer et al., 2011) were used to calculate the We (Eq. 11, σ = 73 mN/m (Klaseboer et al., 2011)), and was compared in Fig. 5 with χ given by Eq. 12. In addition, the numerical data obtained from simulations are added there. As seen, the numerical data and the data calculated on the basis of Eq. 12 (both for values by Legendre et al. (Legendre et al., 2012) and Klaseboer et al. (2011) are in pretty good agreement.
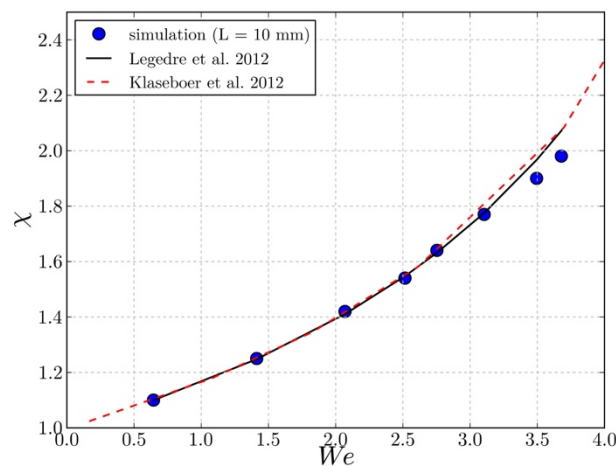
Fig. 5. Comparison of the bubble deformation as a function of Weber number obtained from numerical simulations and taken from literature

The values of drag coefficient as a function of the Reynolds number (Re) are presented in Fig. 6. The data obtained from Eq. 8 using simulated F_D and u_b values (for L = 2 mm) as well as those calculated from the Moore model (Moore, 1965) are compared there. According to the model described by Moore (1965) the drag coefficient of the rising bubble depends on the bubble shape deformation and can be calculated as (Rastello et al., 2011):

$$C_D = \left(\frac{48}{Re}\right) \cdot G(\chi) \cdot \left[1 - 2.21 \cdot \frac{H(\chi)}{\sqrt{Re}}\right] \tag{13}$$

where $G(\chi)$ and $H(\chi)$ are the geometrical factors calculated by Moore (Moore, 1965). The Re is given by:
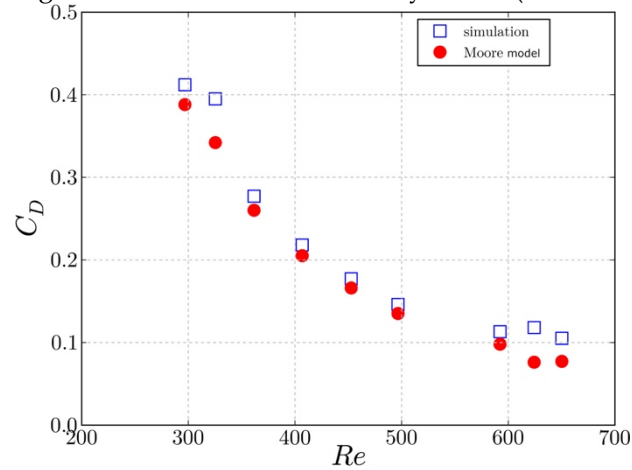
Fig. 6. Drag coefficient exerted on the bubble surface in steady-state conditions compared to theoretical calculations based on the Moore model

$$Re = \frac{2R_b u_b \rho_l}{\mu_l} \tag{14}$$

while the $G(\chi)$ and $H(\chi)$ factors can be accurately approximated by the following relations (Rastello et al., 2011):

$$G(\chi) = 0.1287 + 0.4256\chi + 0.4466\chi^2 \tag{15}$$

$$H(\chi) = 0.8886 + 0.5693\chi + 0.4563\chi^2 \tag{16}$$

As can be seen in Fig. 6 quite good agreement between simulated results and the data calculated according to the Eqs. 13-16 was obtained. The presented data show that the drag coefficient (drag force) increases with decreasing Re value. It means that the drag is higher when the bubble moves slower but also when it is more deformed. In addition, this comparison (Fig. 5 and 6) is a proof of validity of the numerically calculated relations between the bubble rising velocity, deformation and drag force.

Every object (including gas bubble) accelerating in a liquid, experiences drag force related to the work done on the fluid. As a consequence, the apparent mass of the moving body increases and reaches constant value, when steady-state conditions are established. In the case of a rising bubble, it was shown that, for potential flow of inviscid fluid, the added mass (m) of the bubble can be given by the general expression (Brennen, 1982):

$$m = C_m V_b \rho_l \tag{17}$$

where C_m is the added mass coefficient and V_b is volume of the bubble. For a spherical bubble it is well established that the C_m equals 0.5 (Brennen, 1982; Tsao and Koch, 1997; Klaseboer et al., 2001). This situation, however, is encountered only for small bubbles or low Re values. For larger bubbles rising with higher Re, the C_m is a function of bubble surface geometry. It was shown that, in the case of bubbles and drops in an unbounded medium, the added mass coefficient is a function of their axis ratio and can be expressed as (Tsao and Koch, 1997; Klaseboer et al., 2001):

$$C_m = \frac{\alpha}{2-\alpha} \tag{18}$$

with:

$$\alpha = \frac{2\chi^2}{\chi^2-1}\left(1 - \frac{1}{\sqrt{\chi^2-1}} \cdot cos^{-1}\left(\frac{1}{\chi}\right)\right) \tag{19}$$

which, for $1 < \chi < 2.5$, is well-approximated by the linear relation (Klaseboer et al., 2001):

$$C_m = 0.62\chi - 0.12 \tag{20}$$

The kinetic energy of the fluid associated with the motion of the bubble rising with terminal velocity u_b, considering the added mass, can be written as (Harper, 2001; Milne-Thomson, 1968):

$$T = \frac{1}{2}mu_b{}^2 \tag{21}$$

which, after rearrangement and comparison with Eq. 17, allows to compute the C_m for known T and u_b values, according to the relation:

$$C_m = \frac{2T}{\frac{4}{3}\pi R_b{}^3 \rho_l u_b{}^2} \tag{22}$$

Fig. 7 presents the calculated value of C_m as a function of χ on the basis of numerically determined T and u_b values (for steady-state conditions). The data obtained for $L = 2$ and 10 mm are presented there. The solid line refers to the C_m calculated from Eq. 20. As seen, for $L = 10$ mm, i.e. in the case when the influence of proximity of the column walls on the bubble motion could be neglected ($\lambda \rightarrow 1$), the calculated values of C_m (Eq. 22) are practically identical to the theoretical predictions (Eq. 20).
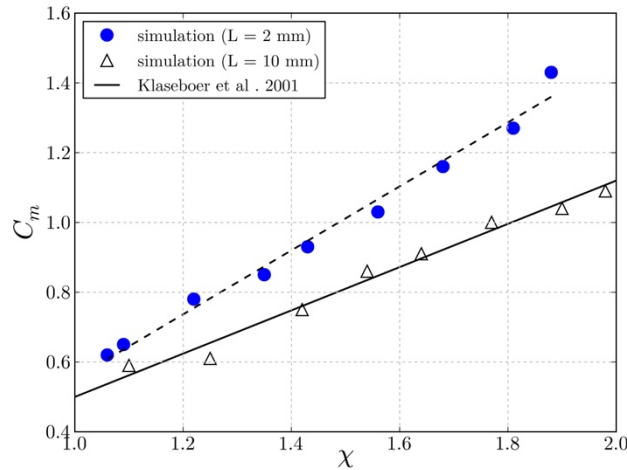
Fig. 7. Calculated added mass coefficient of the bubble as a function of deformation compared with the result of Eq. 20 (Klaseboer et al., 2001)

As was already discussed, the wall proximity influences the added mass of the bubble. It is caused mainly by modification of the kinetic energy of the fluid induced by increase of the drag coefficient. In the case of bubble approaching to the horizontal wall the kinetic energy increases as a result of formation of intervening liquid film, between the bubble and wall interfaces. Recently, Klaseboer et al. (2014) developed the force balance model, where, for the first time, the added mass variations were included in calculations of a rate of liquid film drainage. Creating this model, he considered that the C_m increases during the bubble approach to the solid surface, what influences the inertial force, having significant effect on velocity of drainage of the liquid film. For the sphere, an approximate analytic relation for variations of C_m was given (Klaseboer et al., 2014):

$$C_m(b) = 0.5 + 0.19222\left(\frac{b}{R_b}\right)^{-3.019} + 0.06214\left(\frac{b}{R_b}\right)^{-8.331} + 0.0348\left(\frac{b}{R_b}\right)^{-24.65} + 0.0139\left(\frac{b}{R_b}\right)^{-120.7} \tag{23}$$

where b is the position of the bubble geometrical center in respect to the wall.

Fig. 8 presents the variations of the normalized added mass coefficient of the bubble approaching to horizontal wall with various degree of deformations. The distance of separation is expressed in relation to the bubble radius, as a ratio between b and R_b. The position of the wall was adjusted at $b/R_b = 0$. In addition, the C_m was normalized to the $C_{m\infty}$, i.e. for the added mass coefficient value far away from the wall, where the bubble was rising with terminal velocity (steady-state conditions). Let us analyze the influence of the bubble deformation on C_m variations. These data are illustrated in Fig. 8 by two solid (blue and red) and one short-dashed (green) lines, referring to deformation ratios $\chi = 1.88$, 1.35 and 1.10, respectively. As seen, differences in variations of the C_m are rather small, despite the significant differences in deformation of the approaching bubble. Moreover, all three presented profiles of the C_m variations are quite far from theoretical predictions calculated on the basis of Eq. 23 (black long-dashed line). Even for $\chi = 1.10$, i.e. for the bubble close to sphere, the discrepancy between predictions of Eq. 23 and numerical calculations are significant. It is also interesting to see quite a significant difference between distances from the wall at which the C_m starts to increase for different bubble deformations. As

seen, for $\chi = 1.10$, for which the bubble velocity was the highest, increase of the C_m parameters starts at the $|b/R_b| = 2.8$ and is shifted to ca. 2.2 for higher deformations. This shows directly different timescale of liquid film formation, which is formed "earlier" for the bubble approaching to the wall with higher velocity.

The presented results show that the deformation of the bubble is important parameter for added mass variations in the proximity of the solid wall. The added mass variation is the interplay between bubble deformation and its velocity, which determines the kinetic energy of fluid motion and viscous energy dissipation is a gap between liquid/gas and liquid/solid interface. This, in turn, is crucial for kinetics of drainage of the liquid film formed under dynamic conditions.
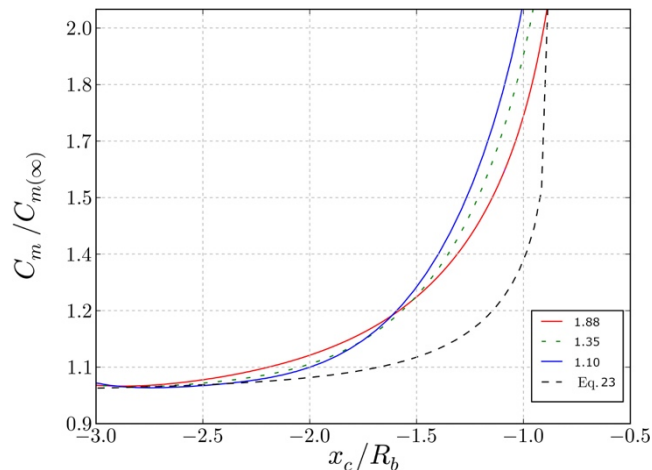
Fig. 8. Normalized added mass coefficient of the bubble of different deformation degrees (see figure legend), approaching to the horizontal no-slip wall

5. Conclusions

On the basis of numerical calculations, influence of the air bubble deformation degree on motion parameters was modeled. It was shown that the bubble deformation can be tuned via proper variations of the Laplace pressure, without changing the bubble radius. The deformation ratio of the bubble was decreased nearly twice (from ca. 1.88 to 1.10) when the Laplace pressure was increased from 54 to 1351 Pa. The velocity of the bubble followed opposite trend, i.e. was increased with increasing pressure values, showing how crucial is the bubble deformation for its hydrodynamics. Approach allowing determination of the added mass coefficient of the bubble, on the basis of bubble motion induced fluid kinetic energy, was proposed and the results of calculations were compared with the literature data. It was shown that the calculation results regarding influence of the bubble deformation on the drag and the added mass coefficients for steady-state conditions, stay in good agreement with theoretical predictions shown earlier in the literature. Additionally, the variations of the added mass coefficient were calculated for the bubble approaching to the horizontal wall. It was shown that increase in the bubble added mass in this case strongly depends on the interplay between (i) bubble deformation degree and (ii) velocity of approach. The influence of these two parameters is strictly connected and should be always considered inseparably. These two factors influence significantly the bubble added mass, and play crucial role in formation and drainage of the liquid film formed under dynamic conditions.

Acknowledgement

References

BIRD, R., STEWART, W., LIGHTFOOT, E., 2007. *Transport Phenomena, (2nd ed.)*. John Wiley and Sons, Inc., New York.

BRENNEN, C., 1982. *A review of added mass and fluid inertial forces*. CR 82.010 Report, Naval Civil Engineering Laboratory, Port Hueneme, 1–50.

CESCHIA M., NABERGOJ, R., 1978. *On the motion of a nearly spherical bubble in a viscous liquid*. Phys. Fluids 21, 140–142.

CLIFT, R., GRACE, J., WEBER, M., 1978. *Bubbles, Drops and Particles*. Academic Press, New York, San Francisco, London. SANGANI, A., ZHANG, D., PROSPERETTI, A., 1991. *The added mass, basset, and viscous drag coefficients in nondilute bubble liquids undergoing small-amplitude oscillatory motion*. Phys. Fluids 3, 2955–2970.

FUSTER, D., AGBAGLAH, G., JOSSERAND, C., POPINET, S., ZALESKI, S., 2009. *Numerical simulation of droplets, bubbles and waves: state of the art*. Fluid Dyn. Res. 41, 065001.

HARPER, J., 2001. *Growing bubbles rising in line*. J. Appl. Math. Dec. Sci. 5, 65–73.

KLASEBOER, E., CHEVAILLER, J., MATE, A., MASBERNAT, O., GOURDON, C., 2011. *Model and experiments of a drop impinging on a immersed wall*. Phys. Fluids 13, 45–57.

KLASEBOER, E., MANICA, R., CHAN, D., KHOO, B., 2011. *BEM simulations of potential flow with viscous effects as applied to a rising bubble*. Eng. Analysis Boundary Elements 35, 489–494.

KLASEBOER, E., MANICA, R., HENDRIX, X., OHL, X., CJAN, D., 2014. *A force balance model of the motion, impact and bounce of bubble*. Phys. Fluids 26, 092101.

KOSIOR, D., ZAWALA, J., MALYSA, K., 2011. *When and how a-terpineol and n-octanol can inhibit the bubble attachment to hydrophobic surfaces*. Physicochem. Probl. Miner. Process, 47, 169-182.

KRISHNA, R., URSCANU, M., VAN BATEN, J., ELLENBERGER, J., 1999. *Wall effect on the rise of single gas bubbles in liquids*. Int. Comm. Heat Mass Transfer 26, 781–790.

KULKARNI, A., JOSHI, J., 2005. *Bubble formation and bubble rise velocity in gas-liquid systems: a review*. Ind. Eng. Chem. Res. 44, 5873–5931.

LEGENRE, D., ZENIT, R., VELEZ-CORDERO, R., 2012. *On the deformation of gas bubbles in liquids*. Phys. Fluids 24 043303.

LEVICH, V., 1962. *Physicochemical Hydrodynamics*. Prentice Hall, Inc., Englewood Cliffs, NJ.

MALYSA, K., 1992. *Wet foams: Formation, properties and mechanism of stability*. Adv. Colloid Interface Sci., 40, 37–83.

MILNE-THOMSON, L., 1968. *Theoretical Hydrodynamics*, (*5th ed.*). Macmillan and Co., LTD, London.

MOORE, D., 1965. The velocity of rise of distorted gas bubbles in a liquid of small viscosity," J. Fluid Mech. 23, 749–766 (1965).

MUKUNDAKRISHNAN, K., QUAN, S., ECKMANN, D., AYYASWAMY, P., 2007. *Numerical study of wall effects on buoyant gas-bubble rise in a liquid-filled finite cylinder*. Physical Review E 76, 036308.

POPINET, S., 2003. *Gerris: a tree-based adaptive solver for the incompressible Euler equations in complex geometries*. J. Comput. Phys. 190, 572–600.

POPINET, S., 2009. *An accurate adaptive solver for surface-tension-driven interfacial flows*. J. Comput. Phys. 228, 5838–5866.

RASTELLO, M., MARIE, J.-L., LANCE, M., 2011. *Drag and lift forces on clean spherical and ellipsoidal bubbles in a solid body rotating flow*. J. Fluid Mech., 682, 434–459.

SIMCIK, M., RUZICKA, M., 2013. *Added mass of dispersed particles by cfd: Further results*. Chem. Eng. Sci. 97, 366–375.

TSAO, H.-K., KOCH, D., 1997. *Observations of high reynolds number bubble interacting with rigid wall*. Phys. Fluids 9, 44–56.

ZAWALA J., DABROS, T., 2013, *Analysis of energy balance during collision of an air bubble with a solid wall*. Phys. Fluids 25, 123101.

ZAWALA, J., 2016. *Energy balance in viscous liquid containing a bubble: rise due to buoyancy*. Can. J. Chem. Eng., 94, 586-595.